Journal of Molecular Structure 1127 (2017) 597–610

Contents lists available at ScienceDirect

Journal of Molecular Structure

journal homepage: http://www.elsevier.com/locate/molstruc

Synthesis, molecular structure, DFT studies and antimicrobial activities of some novel 3-(1-(3,4-dimethoxyphenethyl)-4,5-diphenyl-*1H*-imidazol-2-yl)-1*H*-indole derivatives and its molecular docking studies

D. Rajaraman [a], G. Sundararajan [a], N.K. Loganath [b], K. Krishnasamy [a, *]

[a] Department of Chemistry, Annamalai University, Annmalainagar 608 002, India
[b] Department of Studies and Physics, University of Mysore, Managangothri, India

ARTICLE INFO

Article history:
Received 22 February 2016
Received in revised form
8 August 2016
Accepted 9 August 2016
Available online 11 August 2016

Keywords:
Tetra substituted imidazole
XRD
DFT
Docking
Antimicrobial activity

ABSTRACT

A new series of 3-(1-(3,4-dimethoxyphenethyl)-4,5-diphenyl-1*H*-imidazol-2-yl)-1*H*-indole derivatives (**5a-5j**) are conveniently synthesized and characterized by IR, ^{1}H NMR and ^{13}C NMR spectral techniques. The compound **5f** was also confirmed by single crystal XRD analysis and optimized bond parameters were calculated by density functional theory (DFT) at B3LYP/6–31G (d, p) level. The optimized geometrical parameters obtained by DFT calculation are in good agreement with single crystal XRD data. The experimentally observed FT-IR and FT-Raman bands were assigned to different normal modes of the molecule. The stability and charge delocalization of the molecule were also studied by Natural Bond Orbital (NBO) analysis. The overlapping of atomic orbital along with their predicted energy is explained on the basis of HOMO–LUMO energy gap calculations. Molecular Electrostatic Potential map (MEP) was studied for predicting the reactive sites. The reported molecule used as a potential NLO material since it has high $\mu\beta_0$ value. The antibacterial activities of these derivatives were studied using molecular docking studies and it is compared with their experimental results.

© 2016 Published by Elsevier B.V.

1. Introduction

Imidazole is a class of very important heterocyclic compounds, which can be found in many natural products [1]. They are recognized to exhibit a large variety of important biological and pharmacological activities [2]. It has been reported that some imidazole derivatives can be used as herbicides, fungicides, growth regulators, potent angiotensin II receptor antagonist, glucagon receptor antagonist, anti-allergy, anti-tumor, anti-inflammatory, anti-bacterial, antioxidant and analgesic activities [3–13]. Compounds incorporating the imidazole scaffold are known as inhibitors of interleukin (IL)-1 and 5-lipoxygenase, 20-HETE synthase inhibitors, β-lactamase inhibitors, carboxypeptidase inhibitors, Heme oxygenase inhibitors, NOs inhibitors, p38 MAPK inhibitors, JNK, BRaf kinase, 5-LOX inhibitors and COX-2 inhibitors [14–22]. Imidazole, the N-heterocycle molecule has high electron-withdrawing ability, good coplanarity and good thermal stability which render it to be an ideal building block for nonlinear optical materials [23–25]. Imidazoles are also used as Plant growth regulators and therapeutic agents [26], dye super sensitized star cells (DSSCs) [27,28], nonlinear optics (NLO) [29,30] and organic light emitting diodes (OLED) [31,32]. Vibrational spectroscopy is a valuable tool for the elucidation of molecular structure and gives a dynamical image of the molecule. Vibrational spectroscopy has contributed appreciably to the growth of polymer chemistry, catalysis and reaction dynamics [33]. The present research work predominantly focused on the synthesis of 2-(4-chlorophenyl)-1-(3,4-dimethoxyphenethyl)-4,5-diphenyl-1*H*-imidazole and its FT-IR, FT-Raman vibrational spectral characterizations. To support our experimental investigation, theoretical calculation of vibrational analysis were studied using B3LYP/6-31G (d, p) level of theory [34]. In addition the intramolecular charge transfer, non-linear optical activity, frontier molecular orbital analysis and molecular electrostatic potential of the compound **5f** have been also studied. All the synthesized compounds were evaluated for their antibacterial and antifungal

* Corresponding author. Department of Chemistry, Annamalai University, Annamalainagar, 608 002, Tamilnadu, India.
E-mail address: krishnasamybala56@gmail.com (K. Krishnasamy).

http://dx.doi.org/10.1016/j.molstruc.2016.08.021
0022-2860/© 2016 Published by Elsevier B.V.

screening on different strains of bacteria and fungi.

2. Experimental

2.1. General methods

TLC was carried out to monitor the course of the reaction and the purity of the product. Melting point of the synthesized compounds have been measured in open glass capillaries and were uncorrected **(Cole-Parmer)**. IR spectra were recorded in AVATAR-330 FT-IR spectrophotometer (Thermo Nicolet) and only noteworthy absorption levels (reciprocal centimeters) are listed. The FT-Raman spectrum of the compound **5f** was recorded on BRUKER: RFS27 spectrometer operating at laser 100 mW in the spectral range of 4000–50 cm^{-1}. FT-Raman spectral measurements were carried out from Sophisticated Analytical Instrument Facility (SAIF), Indian Institute of Technology (IIT), Chennai. The ^{1}H and ^{13}C NMR spectra at 400 and 100 MHz, respectively were obtained at room temperature using a Bruker 400 MHz NMR spectrometer (Bruker biospin, California, USA). All the chromatographic purifications were performed with silica gel (100–200 mesh) whereas all TLC (silica gel) was performed on silica gel coated (Merk Kiesel 60 GF 254, 0.2 mm thickness) sheets. All the chemicals and solvents are commercially obtained (Sigma-Aldrich, Merck) and used directly without any further purification.

2.2. Synthesis of 3-(1-(3,4-dimethoxyphenethyl)-4,5-diphenyl-1H-imidazol-2-yl)-1H-indole derivatives

A mixture of aromatic (or) heterocyclic aldehyde (1 mmol), benzil (1 mmol), 2-(3,4-dimethoxyphenyl)ethanamine (1 mmol) and ammonium acetate (2 mmol) with Y_2O_3/SO_4^{2-} (50 mg) as the catalyst [35] was taken in a round bottom flask and the reaction mixture was refluxed at the boiling point of ethanol (78 °C) and the completion of the reaction was monitored by thin layer chromatography (TLC) technique using benzene: ethyl acetate (8:2) as the eluent. The reaction mixture was then extracted with dichloromethane and the resultant material was purified by column chromatography.

2.2.1. 3-(1-(3,4-dimethoxyphenethyl)-4,5-diphenyl-1H-imidazol-2-yl)-1H-indole **(5a)**

White solid: m.p. 157–159 °C and yield 85%. IR (KBr) (cm^{-1}): 1601 (C=N stretching), ^{1}H NMR (δppm): 9.15 (s, NH proton), 7.16–7.87 (m, 15H aryl protons), 6.56 (d, H-12, $J = 8.4$ Hz), 6.20 (d, H-13, $J = 7.2$ Hz), 5.93 (s, H-9), 4.12 (t, H-7, $J = 6.8$ Hz), 3.77 (s, OCH_3), 3.56 (s, OCH_3), 2.47 (t, H-6, $J = 6.8$ Hz), (^{13}C NMR (δppm): 36.06 (C-6), 46.40 (C-7), 55. 89 & 55.60 (OCH_3), 110.99–147.67 (aromatic and ipso carbon), 148.78 (C=N carbon).

2.2.2. 1-(3,4-dimethoxyphenethyl)-4,5-diphenyl-2-(thiophen-2-yl)-1H-imidazole **(5b)**

White solid: m.p. 151–154 °C and yield 89%. IR (KBr) (cm^{-1}): 1608 (C=N stretching), ^{1}H NMR (δppm): 7.12–7.71 (m, 13H aryl protons), 6.66 (d, H-12, $J = 8$ Hz), 6.37 (d, H-13, $J = 1.2$ Hz), 6.13 (s, H-9), 4.18 (t, H-7, $J = 7.2$ Hz), 3.84 (s, OCH_3), 3.78 (s, OCH_3), 2.68 (t, H-6, $J = 7.6$ Hz), ^{13}C NMR (δppm): 36.15 (C-6), 46.50 (C-7), 55. 92 & 55.63 (OCH_3), 111.20–147.88 (aromatic and ipso carbon), 148.96 (C=N carbon).

2.2.3. 1-(3,4-dimethoxyphenethyl)-2,4,5-triphenyl-1H-imidazole **(5c)**

White solid: m.p. 148–151 °C and yield 90%. IR (KBr) (cm^{-1}): 1598 (C=N stretching), ^{1}H NMR (δppm): 7.13–7.98 (m, 15H aryl protons), 6.60 (d, H-12, $J = 8$ Hz), 6.20 (d, H-13, $J = 1.2$ Hz), 6.01 (s, H-9), 4.11 (t, H-7, $J = 7.2$ Hz), 3.85 (s, OCH_3), 3.65 (s, OCH_3), 2.48 (t, H-6, $J = 7.2$ Hz), ^{13}C NMR (δppm): 36.17 (C-6), 46.41 (C-7), 55. 93 & 55.71 (OCH_3), 111.10–147.94 (aromatic and ipso carbon), 148.86 (C=N carbon).

2.2.4. 1-(3,4-dimethoxyphenethyl)-2-(4-(methylthio)phenyl)-4,5-diphenyl-1H-imidazole **(5d)**

White solid: m.p. 156–159 °C and yield 90%. IR (KBr) (cm^{-1}): 1601 (C=N stretching), ^{1}H NMR (δppm): 7.11–7.48 (m, 14H aryl protons), 6.61 (d, H-12, $J = 8$ Hz), 6.24 (d, H-13, $J = 8$ Hz), 6.00 (s, H-9), 4.10 (t, H-7, $J = 6.8$ Hz), 3.81 (s, OCH_3), 3.66 (s, OCH_3), 2.51 (CH_3), 2.47 (t, H-6, $J = 6.4$ Hz), ^{13}C NMR (δppm): 29.74 (CH_3), 36.13 (C-6), 46.53 (C-7), 55. 94 & 55.64 (OCH_3), 111.11–147.83 (aromatic and ipso carbon), 148.88 (C=N carbon).

2.2.5. 1-(3,4-dimethoxyphenethyl)-2-(4-methoxyphenyl)-4,5-diphenyl-1H-imidazole **(5e)**

White solid: m.p. 153–158 °C and yield 92%. IR (KBr) (cm^{-1}): 1597 (C=N stretching), ^{1}H NMR (δppm): 7.12–7.86 (m, 14H aryl protons), 6.97 (d, H-12, $J = 8$ Hz), 6.21 (d, H-13, $J = 8$ Hz), 6.02 (s, H-9), 4.08 (t, H-7, $J = 6.8$ Hz), 3.86, 3.80, 3.68 (s, OCH_3), 2.48 (t, H-6, $J = 6.4$ Hz), ^{13}C NMR (δppm): 55.94, 55.65, 5538 (OCH_3), 36.13 (C-6), 46.46 (C-7), 111.17–147.82 (aromatic and ipso carbon), 148.90 (C=N carbon).

2.2.6. 2-(4-chlorophenyl)-1-(3,4-dimethoxyphenethyl)-4,5-diphenyl-1H-imidazole **(5f)**

White solid: m.p. 160–163 °C and yield 80%. IR (KBr) (cm^{-1}): 1605 (C=N stretching), ^{1}H NMR (δppm): 7.12–7.86 (m, 14H aryl protons), 6.60 (d, H-12, $J = 8.4$ Hz), 6.24 (d, H-13, $J = 2$ Hz), 5.99 (s, H-9), 4.11 (t, H-7, $J = 7.2$ Hz), 3.82, 3.66 (s, OCH_3), 2.46 (t, H-6, $J = 7.2$ Hz), ^{13}C NMR (δppm): 55.94, 55.62 (OCH_3), 36.09 (C-6), 46.58 (C-7), 111.12–147.91 (aromatic and ipso carbon), 148.90 (C=N carbon).

2.2.7. 1-(3,4-dimethoxyphenethyl)-2-(4-fluorophenyl)-4,5-diphenyl-1H-imidazole **(5g)**

White solid: m.p. 157–159 °C and yield 82%. IR (KBr) (cm^{-1})1603 (C=N stretching), ^{1}H NMR (δppm): 7.08–7.89 (m, 14H aryl protons), 6.60 (d, H-12, $J = 8.4$ Hz), 6.24 (d, H-13, $J = 2$ Hz), 5.99 (s, H-9), 4.08 (t, H-7, $J = 7.2$ Hz), 3.81, 3.66 (s, OCH_3), 2.46 (t, H-6, $J = 7.2$ Hz), ^{13}C NMR (δppm): 55.93, 55.62 (OCH_3), 36.06 (C-6), 46.52 (C-7), 111.14–147.88 (aromatic and ipso carbon), 148.88 (C=N carbon).

2.2.8. 4-(1-(3,4-dimethoxyphenethyl)-4,5-diphenyl-1H-imidazol-2-yl)phenol **(5h)**

White solid: m.p. 159–1162 °C and yield 85%. IR (KBr) (cm^{-1}): 1598 (C=N stretching), ^{1}H NMR (δppm): 7.13–7.52 (m, 14H aryl protons), 6.60 (d, H-12, $J = 8.4$ Hz), 6.24 (d, H-13, $J = 2$ Hz), 5.99 (s, H-9), 4.05 (t, H-7, $J = 7.2$ Hz), 3.75, 3.59 (s, OCH_3), 2.43 (t, H-6, $J = 7.2$ Hz), ^{13}C NMR (δppm): 55.94, 55.62 (OCH_3), 36.09 (C-6), 46.58 (C-7), 111.12–147.91 (aromatic and ipso carbon), 148.90 (C=N carbon). 9.8 (s, hydroxyl proton).

2.2.9. 4-(1-(3,4-dimethoxyphenethyl)-4,5-diphenyl-1H-imidazol-2-yl)-N,N-dimethylaniline **(5i)**

White solid: m.p. 160–1163 °C and yield 80%. IR (KBr) (cm^{-1}): 1593 (C=N stretching), ^{1}H NMR (δppm): 7.11–7.52 (m, 14H aryl protons), 6.62 (d, H-12, $J = 8.4$ Hz), 6.29 (d, H-13, $J = 2$ Hz), 6.05 (s, H-9), 4.08 (t, H-7, $J = 7.2$ Hz), 3.80, 3.67 (s, OCH_3), 3.01 $(CH3)_2$, 2.51 (t, H-6, $J = 7.2$ Hz), ^{13}C NMR (δppm): 55.92, 55.66 (OCH_3), 36.15 (C-6), 46.46 (C-7), 40.41 $(CH3)_2$, 111.06–147.69 (aromatic and ipso carbon), 148.83 (C=N carbon).

*2.2.10. 1-(3,4-dimethoxyphenethyl)-2-(4-nitrophenyl)-4,5-diphenyl-1H-imidazole **(5j)***

Yellow solid: m.p. 162–165 °C and yield 79%. IR (KBr) (cm^{-1}): 1603 (C=N stretching), ^{1}H NMR (δppm): 7.26–7.88 (m, 14H aryl protons), 6.60 (d, H-12, $J = 8.4$ Hz), 6.23 (d, H-13, $J = 2$ Hz), 6.05 (s, H-9), 4.19 (t, H-7, $J = 7.2$ Hz), 3.80, 3.67 (s, OCH_3), 3.01 $(CH3)_2$, 2.51 (t, H-6, $J = 7.2$ Hz), ^{13}C NMR (δppm): 55.92, 55.66 (OCH_3), 36.15 (C-6), 46.46 (C-7), 40.41 $(CH3)_2$, 111.06–147.69 (aromatic and ipso carbon), 148.83 (C=N carbon).

2.3. DFT computational method

The density functional theory (DFT/B3LYP) at 6-31G (d, p) level of theory was used to calculate the properties, such as FT-IR, FT-Raman stretching vibrations, optimized geometries, vibrational frequencies, NBO analysis, HOMO-LUMO and hyperpolarizability of the compound **5f**. All the calculations were performed using Gaussian 03 W program package with the default convergence criteria without any constraint on the geometry [36]. The optimized structural parameters were used in the vibrational frequency calculations at the DFT level. The vibrational modes were assigned on the basis of TED (Total Energy Distribution) analysis using SQM program [37]. It should be noted that Gaussian 03 W package able to calculate the Raman activity. The Raman activities were transformed into Raman intensities using raint program [38,39] by the expression:

$$\mathrm{Ii} = \frac{f(\upsilon o - \upsilon i)Si}{\upsilon i\left[1 - \exp\left(-\frac{hc\upsilon i}{KT}\right)\right]}$$

where I_i is the Raman intensity, S is the Raman scattering activities, ν_i is wave number of the normal modes and ν_0 denotes the wavenumber of excitation laser, h, c and k are universal constant and f is a suitably chosen common normalization factor for all peak intensities.

2.4. X-ray crystallographic analysis

The crystal **(5f)** was grown by the slow evaporation technique in ethanol solvent. Diffraction data were collected on a Bruker axs kappa apex2 CCD diffractometer using graphite monochromated Mo Kα radiation (K = 1.54178 Å) at 296 (2) K with crystal size of 0.29 × 0.26 × 0.23 mm. The structure was solved by direct methods and successive Fourier difference synthesis (SHELXS-97) and refined by full matrix least square procedure on F^2 with anisotropic thermal parameters. All non-hydrogen atoms were refined (SHELXL-97) and placed at chemically acceptable positions. A total of 654 parameters were refined with 7171 unique reflections which covered the residuals to $R_1 = 0.0541$. Crystallographic data have been deposited with the Cambridge Crystallographic Data Centre as supplementary publication number CCDC 1419354. Copies of the data can be obtained free of charge via http://www.ccdc.cam.ac.uk or from the Cambridge Crystallographic Data Centre, 12 Union Road, Cambridge CB2 1EZ, UK; fax: +44 1223 336 033: or e-mail: deposit@ccdc.cam.ac.uk.

2.5. Molecular docking study

Molecular docking was carried out to study the exact binding location of ligand on protein. Molecular docking simulation was performed with the Argus Lab 4.0. The prepared 3D structure of 1JIJ protein was downloaded from the protein data bank (see http//www.rcsb.org/pdb) and binding site was made by choosing "Making binding site for this protein" option. The ligand was then introduced and docking calculation was allowed to run using shape-based search algorithm and A Score scoring function. The scoring function is responsible for evaluating the energy between the ligand and protein target. Flexible docking was allowed by constructing grids over the binding sites of the protein and energy based rotation is set for that ligand group of atoms that do not have rotatable bonds. For each rotation, torsions and poses (conformation) are generated during the docking process. For each complex 10 independent runs were conducted and one pose was returned for each run. The best docking model was selected according to the lowest binding energy calculated by Argus lab and the most suitable binding conformation was selected on the basis of hydrogen bond interaction between the ligand and protein near the substrate binding site. The lowest energy poses indicate the highest binding affinity. The resulting receptor model was saved to Brookhaven PDB file from the file the 2D and 3D interactions are viewed in discovery studio 4.5 versions.

2.6. Antimicrobial assay

2.6.1. Collection of bacterial strains

The Clinical isolates of bacterial strains viz., *Staphylococcus aureus, Streptococcus pyogenes, Shigella flexneri, proteus mirabilis* and *vibrio cholera* and the antifungal strains viz., *Candida albicans, Candida glubrate* and *Candida crusei* were used in this study. These strains were obtained from the Department of Botany, Annamalai University, Annamalainagar, Tamil Nadu and India. The strains were inoculated on a sterile medium and sub-cultured on to Mueller Hinton Agar plates, these strains are maintained on agar slant at 4 °C.

2.6.2. Disc diffusion assay

Antibacterial and antifungal activity was performed by the disc diffusion method. About 1 mg/mL stock solution was prepared by dissolving the test compounds (**5a-5j**) in 50% DMSO. The sterile paper disc with 6 mm diameter was impregnated with concentration of 200 mg/mL and the discs were placed in Mueller Hinton Broth for bacteria and Sabourauds dextrose broth for fungi. The plates were incubated at 37 °C for bacteria and 28 °C for fungi in incubator. The zone of inhibition for bacteria was visually examined at 37 °C for 24 h and fungi was visually examined at 28 °C for 72–96 h. Methicillin was used as a standard positive control for bacteria and Amphotericin B was used as a standard positive control for fungi under analogues conditions. All the tests were carried out in triplicate.

2.6.3. Minimum inhibitory concentration (MIC)

Dilution susceptibility testing method was used for MIC determination. The test compounds were dissolved in 1 mL of chloroform. The different concentrations of the test compounds were 200–3.125 μg/mL. It was then serially diluted in to two folds. Wherein, 100 mL of sterile Mueller Hinton Broth for bacteria and Sabourauds Dextrose broth for fungus was decanted into each well of a sterile 96-well micro plate. Highest concentration of the test compounds added at 100 mL to the first well. After mixing of the above, 100 mL of the same was transferred to the second well and in this way; the dilution procedure was continued as a series of dilution of 200–3.125 μg/mL respectively. Inoculums solution at 5 mL was added to every well. Being incubated for 24 h at 37° C for bacteria and 28 °C for fungi, the tubes were monitored for turbidity as growth and non-turbidity as no growth. The MIC values were interpreted as the highest dilution (lowest concentration) of the sample, which showed clear fluid with no development of turbidity. Bacterial and fungal growth was indicated by the measure of a white pellet on well bottom.

3. Results and discussion

3.1. Chemistry

One-pot processes for the synthesis of the title compounds (**5a**–**5j**) are sketched in Scheme 1. The novel 3-(1-(3,4-dimethoxyphenethyl)-4,5-diphenyl-1*H*-imidazol-2-yl)-1*H*-indole derivatives were prepared using one pot multicomponent reaction by condensing benzil, various aromatic and heterocyclic aldehydes, 2-(3,4-dimethoxyphenyl)ethanamine and ammonium acetate in 1: 1: 1:2 ratio in the presence of sulphated yttria. A plausible mechanism [40] for the SO_4^{2-}/Y_2O_3 catalyzed synthesis of substituted imidazole has been proposed through Scheme 2. In the case of 1,2,4,5-tetrasubstituted imidazole, the reaction proceeds via a diamine intermediate **A**, which is formed by the activation of aldehydic carbonyl group by the SO_4^{2-}/Y_2O_3 catalyst through intermolecular hydrogen bonding and the condensation of diamine with benzil followed by dehydration to form the imino intermediate **B**, which rearranges to form the desired product **C**. The representative compound **5a** was characterized by IR, ^1H, ^{13}C NMR and 2D NMR (HSQC) spectral techniques. Compound **5f** was successfully crystallized and its structure was determined by single-crystal X-ray diffraction analysis. In the IR spectrum of compound **5a**, the strong band obtained at 3251 cm^{-1} was due to NH band of the indole group. The strong absorption band at 1601 cm^{-1} was due to imidazole ring containing C=N. In the ^1H NMR spectrum of **5a** there was a singlet at 9.38 ppm corresponding to one proton. This is due to the NH proton of the indole group. There was a multiplet in the region of 7.16–7.87 ppm, corresponding to 15 protons and it is due to aromatic protons. There are two doublets in the region at 6.56 and 6.20 ppm, each corresponding to one proton. These are due to the H-13 and H-12 protons. There was one singlet at 5.93 ppm. These are due to H-9 proton. There was two triplets at 4.10 (H-6) and 2.47 ppm (H-7) ppm, corresponding to two methylene protons. There were two singlets at 3.77 and 3.56 ppm corresponding to two methoxy group. In the ^{13}C NMR spectrum of compound 5a, the signal appeared at 148.78 ppm is unambiguously

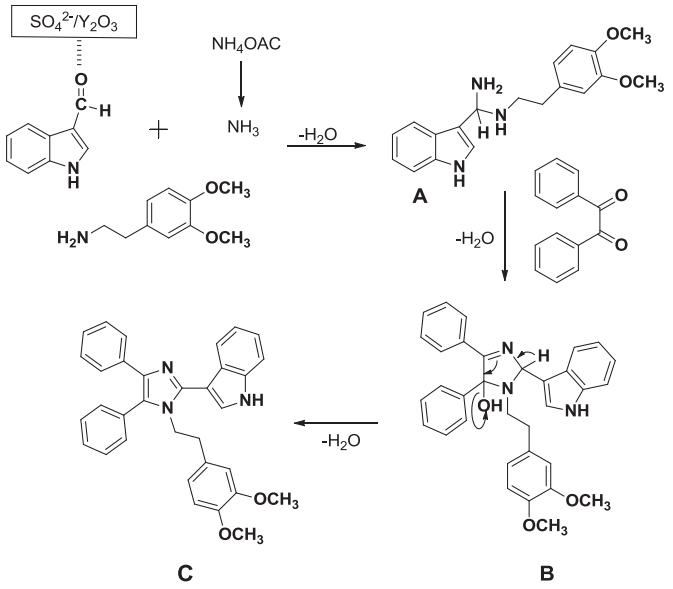

Scheme 2. Plausible mechanism for the formation of the product **5a**.

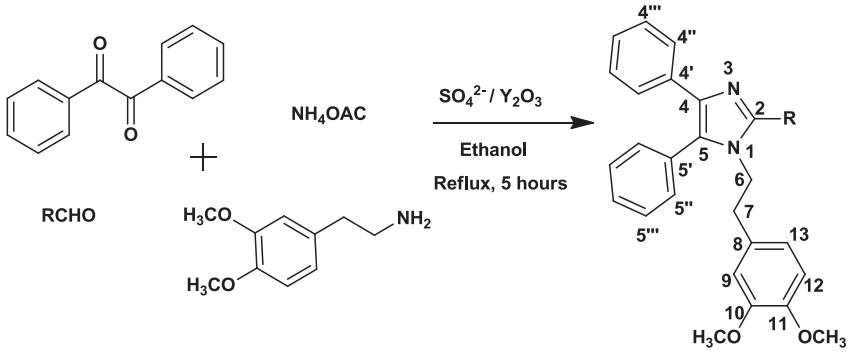

Compounds	Entry	R	Compounds	Entry	R
	5a			5f	Cl
	5b			5g	F
	5c	H_3CS		5h	HO
	5d			5i	H_3C, N, H_3C
	5e	H_3CO		5j	O_2N

Scheme 1. Synthesis of 3-(1-(3,4-dimethoxyphenethyl)-4,5-diphenyl-*1H*-imidazol-2-yl)-*1H*-indole derivatives.

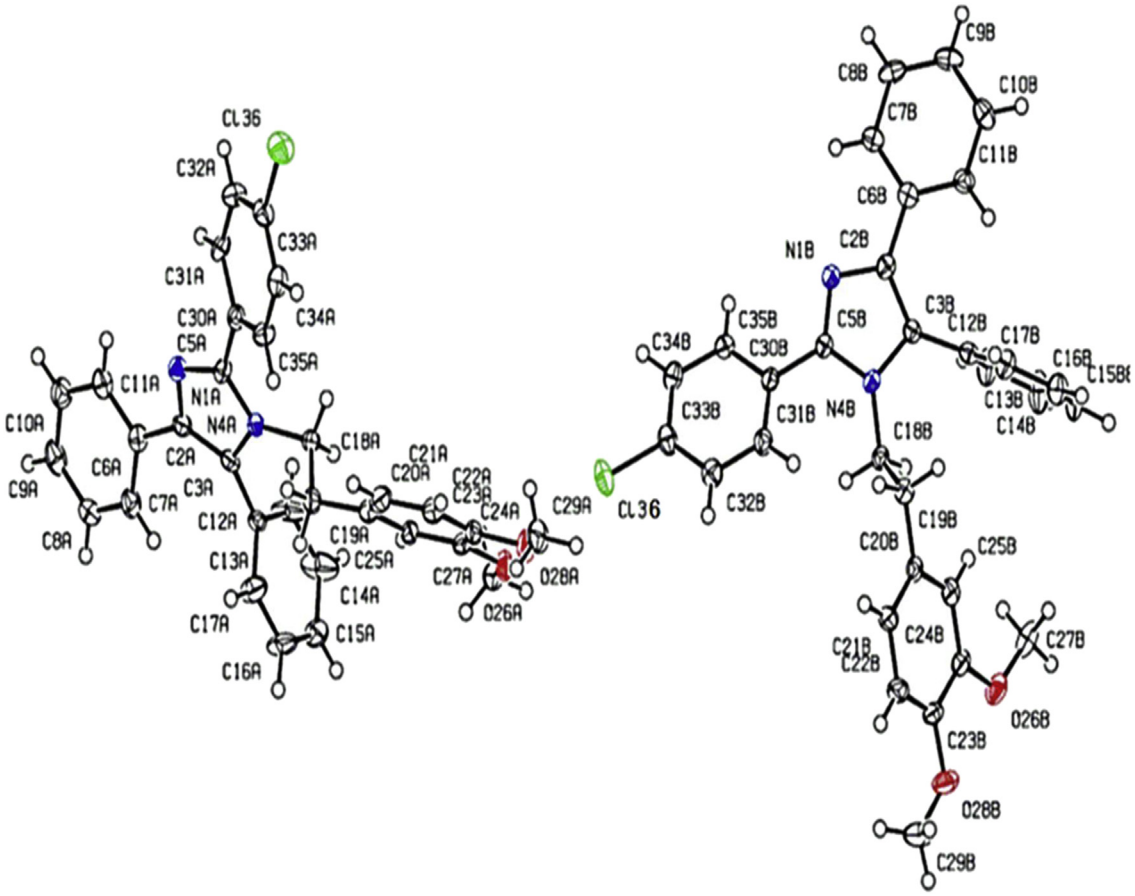

Fig. 1. ORTEP of compound **5f.**

assigned to imino (C═N) carbon of the imidazole ring (C-2). The aromatic carbon signals are appeared in the region of 147.67–110.99 ppm. The signals observed at 55.89 and 55.60 ppm are assigned to two methoxy carbons. The signals observed at 36.06 and 46.40 ppm are assigned to C-6 and C-7 carbons respectively. In $^{1}H-^{13}C$ COSY spectrum of **5a,** the carbon signals at 148.78 ppm does not have HSQC correlation confirmed that the signal is due to imino carbon (C-2). The H-6 ($\delta = 4.10$ ppm) and H-7 ($\delta = 2.47$ ppm) protons have cross peak with corresponding carbon signals at 36.06 and 46.40 ppm this is due to C-6 and C-7 carbons. This observation confirmed that the formation of two methylene protons. Further, the signals at 3.77 and 3.56 ppm in methoxy proton have cross peak with corresponding carbon signals at 55.89 and 55.60 ppm. The aromatic proton signals have cross peak with corresponding carbon signals except ipso carbons. The ^{1}H, ^{13}C NMR and HSQC correlation spectrum of compound **5a** is shown in Supplementary information S1 (Fig. 1).

3.2. Crystal and molecular structure of *5f*

Single crystal X-ray diffraction analysis has been performed for 2-(4-chlorophenyl)-1-(3,4-dimethoxyphenethyl)-4,5-diphenyl-*1H*-imidazole **(5f)** and its crystal data, structure refinement parameters are given in Table 1. The ORTEP indicated that the compound **5f** is crystallized with two independent asymmetric units are shown in Fig. 1. The single crystal X-ray crystallography determination reveals that the compound **5f** crystallized in orthorhombic system with space group *Pca*21 with cell dimensions of a = 11.2902 (3)Å, b = 21.436 (6) Å and c = 21.1041 (5) Å. In compound **5f**, the imine C5═N1 and amine C5–N4 bond distances are 1.32 (5) and 1.35 (5) Å. The selected bond distances are C2–C3 1.37 (6) Å, N4–C3 1.40 (5) Å, N1–C2 1.38 (5) Å, Cl36–C33 1.75 (4) Å, O26–C24 1.36 (5) Å and O28–C23 1.37 (5) Å. The selected dihedral

Table 1
Crystal data and structure refinement details of **5f**.

Parameters	5f
Empirical formula	C31H27 Cl N2 O2
Formula weight	495.01
Temperature(T)	296(2) K
Wavelength	1.54 Å
Crystal system, space group	orthorhombic, *Pca*21
Unit cell dimensions	a = 11.2902 (3)Å alpha = 90° b = 21.436 (6) Å beta = 90° c = 21.1041 (5) Å gamma = 90°
Volume	5102.21 Å
Z	8
Absorption coefficient	1.568mm-1
F(000)	2080
Crystal size	0.29 × 0.26 × 0.23 mm
Theta range for data collection	2.06–64.40 deg.
Completeness to theta = 25.00	100.0%
Absorption correction	Semi-empirical from equivalents
Max. and min. transmission	0.652 and 0.71
Refinement method	Full-matrix least-squares on F^2
Data/restraints/parameters	7171/1/654
Goodness-of-fit on F^2	1.025
Final R indices [I > 2sigma(I)]	R1 = 0.0541, wR2 = 0.1252
R indices (all data)	R1 = 0.0646, wR2 = 0.1317
CCDC NO	**1419354**

Table 2
Selected bond length, bond angle and dihedral angle of **5f**.

Bond length	Exp	Theoretical	Dihedral angle	Exp	Theoretical
C2–C3	1.37(6)	1.39	C27–O26–C24–C23	−179.1(4)	−175.85
Cl36–C33	1.75(4)	1.55	C27–O26–C24–C25	1.2(6)	57.53
O26–C24	1.36(5)	1.39	C24–O26–C27–H27	179.1	176.67
O26–C27	1.43(6)	1.46	C29–O28–C23–C24	−178.4(4)	−178.55
O28–C23	1.37(5)	1.45	C29–O28–C23–C22	1.1(6)	3.46
O28–C29	1.44(6)	1.39	C23–O28–C29–H29	−58.5	–
N4–C5	1.35(5)	1.39	C18–N4–C5–N1	174.1(3)	173.08
N4–C18	1.46(5)	1.47	C18–N4–C5–C30	−2.6(6)	−7.01
N4–C3	1.40(5)	1.40	C3–N4–C5–N1	0.1(4)	173.08
N1–C5	1.32(5)	1.33	C3–N4–C5–C30	−176.6(4)	179.25
N1–C2	1.38(5)	1.38	C5–N4–C18–H18	−19.1	62.37
Bond angle			C5–N4–C18–C19	102.2(4)	−9.45
C24–O26–C27	116.9(3)	118.46	C3–N4–C18–H18	36.7	−124.8
C23–O28–C29	116.2(3)	116.63	C3–N4–C18–C19	−84.6(4)	111.65
C5–N4–C18	128.8(3)	128.68	C5–N4–C3–C12	177.1(4)	−177.23
C5–N4–C3	107.2(3)	106.06	C5–N4–C3–C2	−0.3(4)	0.35
C18–N4–C3	123.7(3)	124.00	C18–N4–C3–C12	2.7(6)	8.67
C5–N1–C2	105.0(3)	107.00	C18–N4–C3–C2	−174.7(3)	−173.73
O26–C24–C23	116.5(4)	123.12	C2–N1–C5–N4	0.1(4)	0.65
O26–C24–C25	123.4(4)	117.24	C2–N1–C5–C30	176.9(4)	−179.25
O28–C23–C24	115.8(4)	118.17	C5–N1–C2–C6	−179.5(4)	178.88
O28–C23–C22	124.4(4)	116.63	C5–N1–C2–C3	−0.3(4)	−0.41
N4–C5–N1	112.1(3)	110.13	O26–C24–C23–O28	−0.5(5)	−2.93
N4–C5–C30	124.3(3)	128.31	O26–C24–C23–C22	−179.9(4)	176.67
N1–C5–C30	123.4(4)	121.55	C25–C24–C23–O28	179.2(4)	−178.55
N4–C18–H18	109	109.41	O26–C24–C25–H25	−1.3	3.46
N4–C18–C19	112.9(3)	106.55	O26–C24–C25–C20	178.7(4)	−175.85
O26–C27–H27	109.5	117.14	O28–C23–C22–H22	1	0.8
O28–C29–H29	109.5	123.12	O28–C23–C22–C21	−179.0(4)	−178.55
N4–C3–C12	120.7(3)	122.14	C17–C12–C3–N4	86.4(5)	91.75
N4–C3–C2	104.6(3)	110.13	C13–C12–C3–N4	−90.2(5)	−88.34
Cl36–C33–C32	119.9(3)	119.23	N4–C18–C19–C20	−174.7(3)	−64.57
Cl36–C33–C34	118.6(3)	119.14	N4–C18–C19–H19	−53.7	−63.96
			N4–C18–C19–H19	64.4	174.10
			H32–C32–C33–Cl36	0.3	1.05
			H34–C34–C33–Cl36	−0.7	−0.30
			C35–C34–C33–Cl36	179.5(3)	−179.76
			N4–C3–C2–N1	0.3(4)	0.02
			N4–C3–C2–C6	179.5(4)	−179.17
			C12–C3–C2–N1	−176.4(4)	177.28

angles of the molecules are C6–C2–C3–C12 2.7 (8)°, N4–C8–C19–C20–174.7 (3)°, C2–N1–C5–C30 176.9 (4)°, C5–N1–C2–C6 -179.5 (4)° and N4–C18–C19–C20–174.7 (3)°. The imine (C=N) bond length is expected to be shorter than the amine (C–N) bond length. The selected bond length, bond angle and dihedral angle are listed in Table 2. These data revealed that the two phenyl rings at C2 and C5 are lying in the same plane as that of the imidazole ring system, while phenyl rings at C3 and 2-(3,4-dimethoxyphenyl)ethyl ring system N4 are deviated from the planarity with an angle of −160.5 (C7–C6–C2–N1) and 173.4 (C3–C12–C13–C14) respectively. A unit cell contains eight molecules in the Packing diagram of compound **5f** is shown in Fig. 2. The experimental single crystal structural parameters (bond length, bond angle and dihedral angle) of compound **5f** are compared with theoretical bond parameters. It shows substitution in aromatic ring does not affect notably in bond parameters. The optimized preferred bond parameters are given in Table 2. All the bond parameters are excellent agreement with XRD values. The optimized structure of compound **5f** is shown in Fig. S2 (Supplementary information).

3.3. Vibrational analysis

The synthesized compound **5f** is subjected to IR and Raman spectral analysis and the observed and theoretical FT-IR spectrum is given in Fig. 3 and the observed and theoretical FT-Raman spectrum

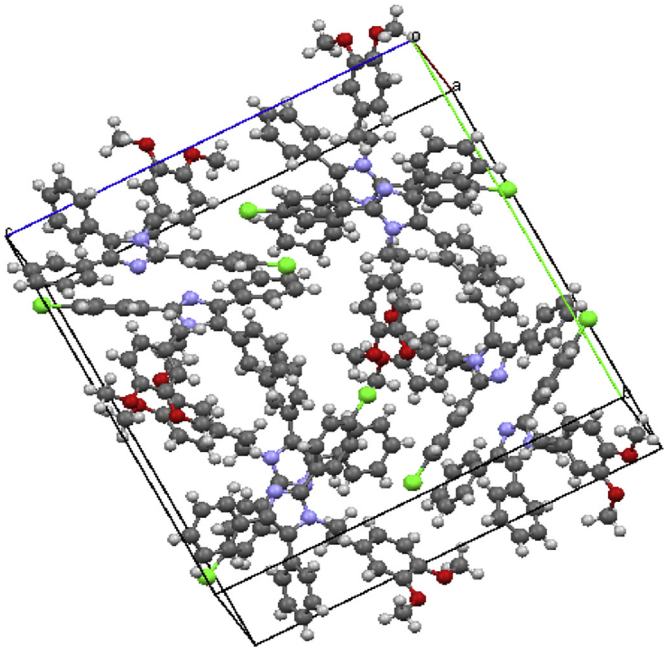

Fig. 2. Packing diagram of **5f**.

is given in Fig. 4. The selected vibrational wavenumber of the compound **5f** are analyzed using DFT/B3LYP 6-31G (d, p) Table 3 and the all the vibrational wavenumber are given in S1 (Table 1. Supplementary information). The theoretical vibrational frequencies are found to be in good agreement with the observed vibrational frequencies. The normal modes assignment of the theoretical IR frequencies is visualized and substantiated with the help of the Gauss view 5.0 visualization programs. The synthesized **5f** consists of 63 atoms and hence has 183 normal modes of vibrations which include 62 stretching, 123 in-plane bending and 60 out-of-plane bending vibrations. Scaling factor values [41] of 0.96 used for C–H, C-X stretching, bending, wagging, ring puckering and torsion vibrational [42] frequencies, respectively. The molecule **5f** belongs to C1 symmetry.

3.3.1. C–H modes

The aromatic C–H stretching vibrations are normally found between 3100 and 3000 cm^{-1} [43]. In compound **5f**, the C–H modes were calculated in the range of 3038–3251 cm^{-1} (mode nos: 157 to 183) Most of these calculated frequencies find a correlation with the strongly observed infrared and Raman bands in the range 3118–2849 cm^{-1}& 3175-3050 cm^{-1}.

3.3.2. CH_2 modes

The asymmetric and symmetric CH_2 stretching vibrations are normally appear in the region 3100-2900 cm^{-1} [44]. The calculated CH_2 bending modes were assigned to the bands at 1536, 1537, 1550, 1560 1562 cm^{-1} and 1475, 1477, 1489, 1499, 1501 cm^{-1} in FT-IR and FT- Raman (mode nos: 141 to 146). The experimental CH_2 bending modes were assigned to the bands at 1478, 1501 cm^{-1} and 1387, 1418, 1518, 1557 cm^{-1} in FT-IR and FT-Raman were in good agreement with the data.

3.3.3. C=N modes

The C=N vibration normally appears in the region of 1471–1689 cm^{-1} [45]. The strong band observed at 1610 cm^{-1} in the experimental IR spectra (1601 cm^{-1} in FT-Raman) of **5f** is assigned to C=N vibration. The mode no 137 with the scaled frequency1451 cm^{-1} visualizes the C=N stretching.

3.3.4. C–Cl modes

The vibrations due to the halogen atom attached to aromatic ring are significance to discuss here, Mooney assigned vibrations of C-X group (X = Cl, Br and I) in the frequency range 1129–480 cm^{-1} [46]. In present study C–Cl stretching vibration was observed at 435 and 410 cm^{-1} in FT-IR and FT-Raman and was in good agreement with the theoretically calculated value 421 and 405 (mode no 35).

3.3.5. C–N and C–O modes

The identification of C–N vibration is a very difficult task, since mixing of several bands are possible in this region. However, with the help of theoretical calculation B3LYP 6-31G (d, p) the C–N stretching vibrations are calculated. In this study, the band at 1148 cm^{-1} in FTIR spectrum is assigned to C–N stretching vibration. In the present investigation the calculated N4–C1 stretching

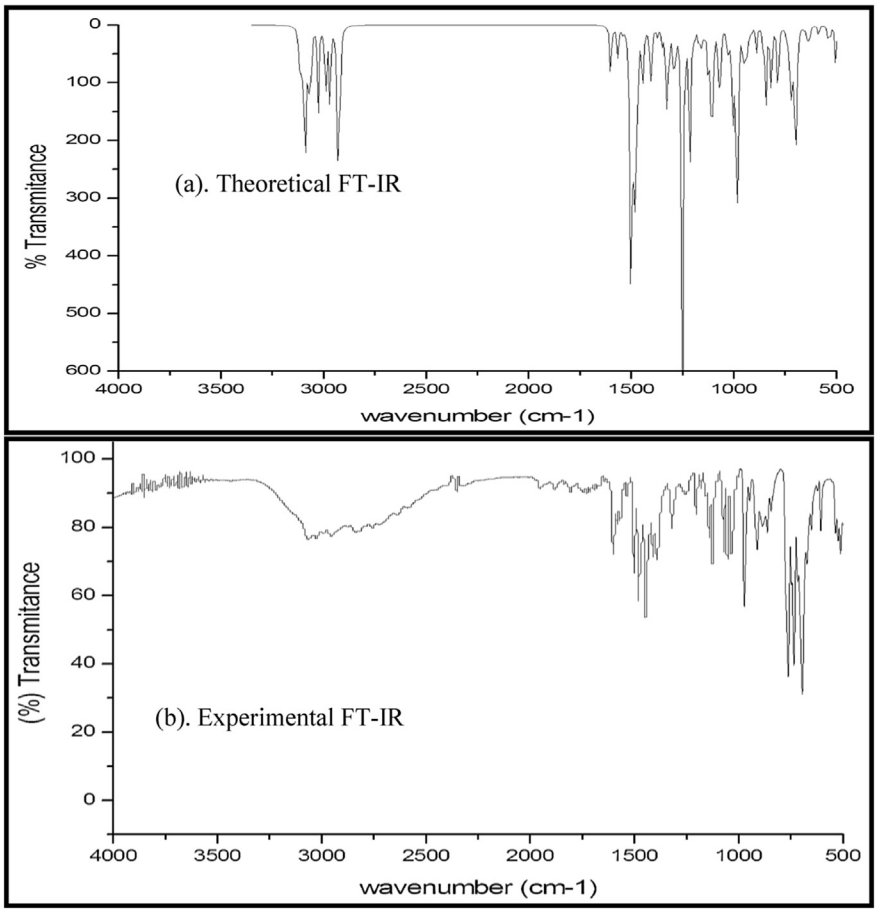

Fig. 3. Combined Theoretical FT-IR (a) and Experimental FT-IR (b) spectrum of compound **5f.**

vibration appeared at 1249 and 1200 cm^{-1} in FT-IR and FT-Raman (mode no: 113) show excellent agreement with experimental data. The C–O stretching vibrations are calculated at the range of 890–855 cm^{-1} & 1020-980 cm^{-1} (mode no: 73 and 85) and observed stretching vibrations appeared at 1070 & 910 cm^{-1} and 826 & 996 in FT-IR and FT-Raman were in good agreement with the data.

3.4. HOMO–LUMO energy

The analysis of the wave function indicates that the electron absorption corresponds to the transition from the ground state to the first excited state is mainly described by one electron-excitation from the highest occupied molecular orbital (HOMO) to the lowest unoccupied molecular orbital (LUMO) [47]. LUMO as an electron acceptor represents the ability to obtain an electron and HOMO as an electron donor represents the ability to donate electron. The energy gap between the HOMO and LUMO molecular orbital determine the chemical stability and electrical transport properties of molecule. The red and green colors of the molecular orbital plot represent the positive and negative phase respectively. The HOMO shows the charge density localized over the imidazole and the entire phenyl ring except hydrogen. The LUMO part is located on imidazole and except 2-(3,4-dimethoxyphenyl)ethyl ring. The energy difference between the HOMO and LUMO is about 4.38eV. The smaller band gap energy increases the stability of the molecule. The frontier molecular orbital of **5f** (HOMO–LUMO) are shown in Fig. 5.

3.5. NBO analysis

In natural Bond Orbital (NBO) analyses several donor-acceptor interactions are observed in compound **(5f)** and among the strongly occupied NBOs, the most important delocalization sites are in the p system and in the lone pairs (n) of the oxygen and nitrogen present on the imidazole and dimethoxy moiety. The s system shows some contribution to the delocalization and almost the donor-acceptor interactions are same in these compound. The most important interaction energies of charge transfer are mainly by the orbital overlap between n (LP- N4) and π*C5–N1 with stabilization energy 197.86 kJ/mol and electron density 1.55e. These bonds orbital which results intramolecular charge transfer (ICT) causing stabilization of the system. The π-π* electron transitions are more favorably operated between Πc30-C35 → π*C33–C34, πC31- C32 → π*C33–C34 and πC15-C16 → π*C12–C17 which is stabilized by 92.63, 90.83 and 90.33 kJ/mol. These interactions are observed as an increase in electron density (ED) in C–C anti-bonding orbital that weaken their respective bonds [48]. In NBO analysis large $E^{(2)}$ values shows the intensive interaction between electron-donors and electron acceptor interaction. The possible intensive interactions are given in S2. (Table 2. Supplementary Information).

3.6. Molecular electrostatic potential (MEP)

Molecular electrostatic potential provides a visual method to understand the relative polarity of the molecule. MEP is in valuable

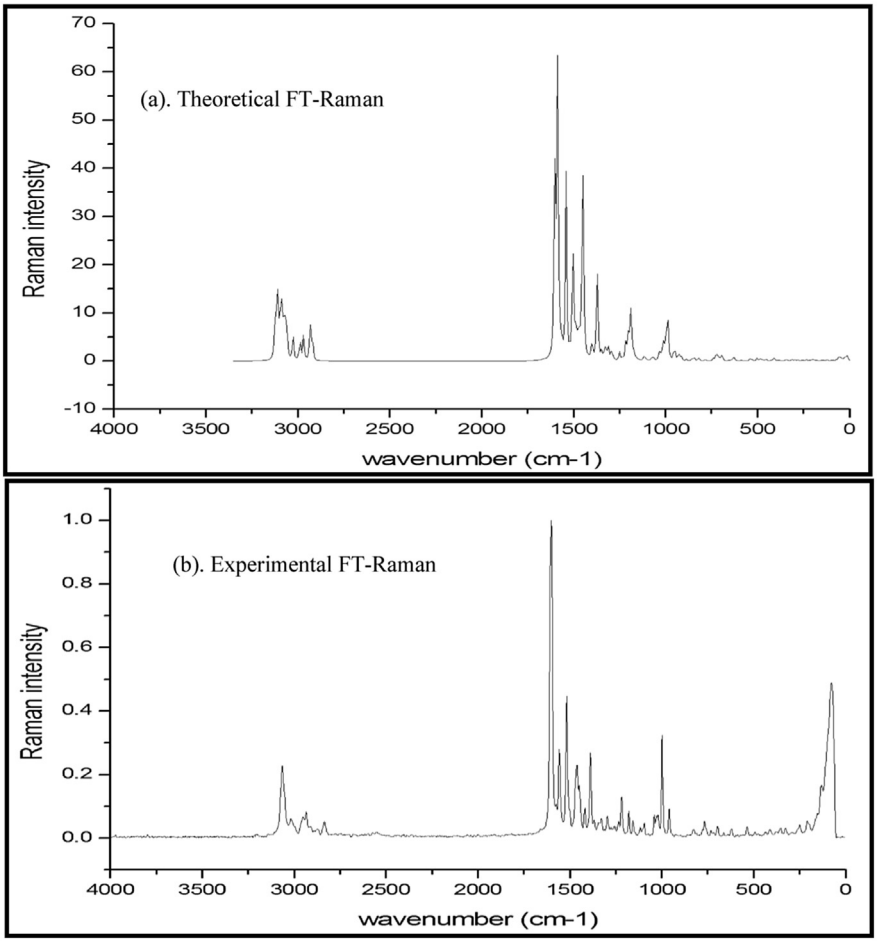

Fig. 4. Combined Theoretical FT-Raman (a) and Experimental FT-Raman (b) spectrum of compound **5f.**

tool in predicting and analyzing the molecular interactions such as Drug − receptor and enzyme − substrate interactions. MEP is very helpful for the qualitative elucidation of electrophilic and nucleophilic reactions for the study of biological discovery process and hydrogen bonding interactions [49]. An electron density iso-surface mapped with electrostatic potential surface depicts the size, shape, charge density and site of chemical reactivity of the molecule. The different values of the electrostatic potential at the surface are represented by different colors; the red color surfaces with negative MEP are due to high electron density. The blue color surfaces are due to lowest electron density. MEP map with electron contour graph of **5f** is shown in S3 (Fig. 3. Supplementary Information). The MEP shows that the negative potential site is situated over imidazole and (C-2) phenyl group and the positive potential site are present around the hydrogen atoms. The regions over the rings are neutral and it is represented by green color. These sites given information about the region from where the molecule can have intermolecular interactions [50].

3.6.1. Mulliken and NBO charge analyses

The calculation of atomic charges plays an important role in the application of quantum mechanical calculations to molecular systems [51]. The total atomic charge values are obtained by Mulliken population analysis with optimized geometry and natural charges are obtained by Natural Bond Orbital analysis (NBO) and its data are listed in S3 (Table 3. Supplementary Information). As seen in from Table S2, the two methods predict the same tendencies. The C3and C52 atoms has higher positive atomic charges (0.27 (Mulliken); 0.35 (NBO)) and (0.27 (Mulliken); 0.25 (NBO)) than the other carbon atoms. This is due to the electronegative atoms such as oxygen and nitrogen attached to carbon atoms. Results from Table S2, oxygen and nitrogen atoms in compound **5f** have more negative charges than the other atoms. Mulliken and NBO Population methods are predicting the reactive sites present in compound **5f**. According to these result, NBO's net charges are slightly larger than Mulliken charges, which is also supported by MEP analysis.

3.7. Nonlinear optics (NLO)

The hyperpolarizability (β_0), dipole moment (μ) and polarizability (α_0) is calculated using B3LYP/6-31G (d, p) on the basis of the finite-field approach. The calculated polarizability and hyperpolarizability are reported in electrostatic units (e.s.u) and the values are presented in Table 4. The large value of hyperpolarizability (β_0) which is a function of the non-linear optical activity of the molecular system is associated with the intramolecular charge transfer, resulting from the electron cloud movement through conjugated framework from electron donor to

Table 3
Selected vibrational wavenumbers obtained for **5f** at B3LYP/6-31G (d, p).

Number of modes	Calculated frequencies (cm^{-1})		Observed frequncies (cm^{-1})		IR intensity		Raman intensity		Vibrational assignment (PED)
	Un scaled	Scaled	FT-IR	FT-Raman	Abs.	Rel.	Abs.	Rel.	
35	421	405	435	410	8.01	3.32	52.9	0.88	$\upsilon C_{33}Cl_{36}(45)$
52	662	636		619	4.35	1.80	24.9	0.42	$\upsilon N_4C_{18}(11)+\beta C_8C_9C_{10}(46)$
73	890	855	910	826	7.44	3.08	14.9	0.25	$\upsilon O_{26}C_{24}(45)$
85	1020	980	1070	996	77.48	32.12	22.3	0.37	$\upsilon O_{28}C_{23}(65)$
113	1249	1200		1218	2.35	0.97	479.7	7.97	$\upsilon N_1C_2(31)$
117	1301	1250		1387	241.2	100.0	105.2	1.75	$\upsilon C_{20}C_{21}(57)+ \upsilon O_{28}C_{23}(19)+ \upsilon O_{59}C_{52}(40)+ \beta H_{22}C_{22}C_{23}(59)$
129	1427	1371			1.09	0.45	708.3	11.7	$\upsilon N4C3(10)+TORSH_{18}C_{18}N_4C_3(24)$
137	1511	1451	1610	1601	2.61	1.08	2162	35.95	$\upsilon N_1C_5(44)+ \beta H_{35}C_{35}C_{34}(46)$
141	1537	1477	1478	1418	15.79	6.55	93.0	1.55	$\beta H_{19}C_{19}H_{19}$ (83)
143	1550	1489	1501	1518	33.07	13.71	210.9	3.51	$\beta H_{18}C_{18}H_{18}(70)$
145	1560	1499		1557	46.75	19.38	130.2	2.16	$\beta H_{22}C_{22}C_{23}(79)$
146	1562	1501			66.48	27.56	30.65	0.51	$\beta H_{22}C_{22}C_{23}$ (59)
157	3038	2919	3023	2834	43.11	17.87	55.54	0.92	$\upsilon C_{31}H_{31}(99)$
158	3049	2929			71.93	29.82	63.85	1.06	$\upsilon C_{35}H_{35}(99)$
159	3052	2933	3063	2934	22.98	9.53	56.19	0.93	$\upsilon C_7H_7(86)$
160	3090	2969	3089		45.38	18.81	82.44	1.37	$\upsilon C_6H_6(87)$
161	3109	2987	3109		11.37	4.71	33.95	0.56	$\upsilon C_{22}H_{22}(99)$
162	3112	2990	3111		35.72	14.81	21.95	0.36	$\upsilon C_{10}H_{10}(87)$
163	3149	3025		3016	37.70	15.63	40.11	0.67	$\upsilon C_{23}H_{23}(99)$
164	3149	3026	3149		6.81	2.82	20.79	0.35	$\upsilon C_{13}H_{13}(97)$
165	3183	3058			18.39	7.62	55.53	0.92	$\upsilon C_8H_8(94)$
166	3186	3061	3186		0.91	0.38	21.38	0.36	$\upsilon C_{16}H_{16}(93)$
167	3189	3064	3188	3063	12.56	5.21	35.61	0.59	$\upsilon C_{25}H_{25}(82)$
168	3194	3069	3194		0.57	0.24	19.62	0.33	$\upsilon_{C21}H_{21}(98)$
169	3197	3071		3070	23.37	9.69	63.16	1.05	$\upsilon C_{15}H_{15}(99)$
170	3205	3079	3205	3078	8.13	3.37	53.30	0.89	υC_8H_8 (87)
171	3209	3083	3209	3082	6.87	2.85	22.76	0.38	$\upsilon C_{15}H_{15}(93)$
172	3215	3089			49.66	20.59	97.11	1.61	$\upsilon C_{27}H_{27}(83)$
173	3215	3089			22.50	9.33	42.46	0.71	υ $C_{10}H_{10}(98)$
174	3215	3089	3215	3088	5.39	2.23	23.82	0.40	υ $C_{29}H_{29}(92)$
175	3224	3097		3097	29.05	12.04	73.60	1.22	υ $C_{27}H_{27}(100)$
176	3231	3104	3230		5.97	2.48	21.70	0.36	υ $C_{18}H_{18}(97)$
177	3233	3107		3107	0.96	0.40	32.50	0.54	υ $C_{29}H_{29}(88)$
178	3236	3109	3236	3109	4.81	1.99	79.37	1.32	υ $C_{19}H_{19}$ (93)
179	3238	3111	3238		7.73	3.21	37.71	0.63	υ $C_{18}H_{18}(89)$
180	3241	3114		3113	8.28	3.43	15.58	0.26	υ $C_{19}H_{19}(97)$
181	3245	3118	3244	3117	5.16	2.14	55.55	0.92	υ $C_{19}H_{19}(89)$
182	3248	3120		3119	9.39	3.89	7.71	0.13	$\upsilon C_{27}H_{27}(97)$
183	3251	3123	3250		0.73	0.30	78.14	1.30	$\upsilon C_{29}H_{29}(94)$

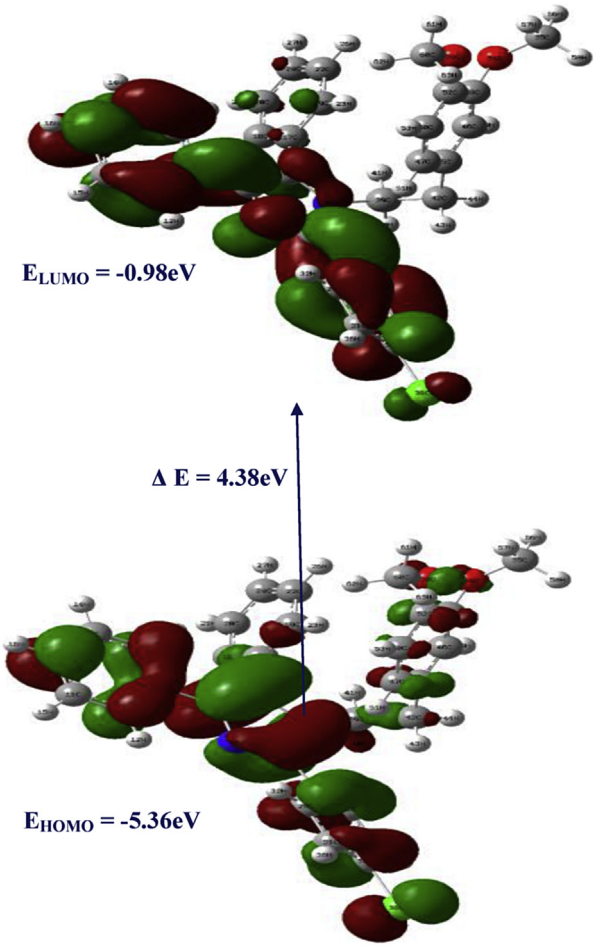

Fig. 5. HOMO-LUMO energy diagram of **5f.**

Table 4
The molecular electric dipole moments μ (Debye), Polarizability (α_0) and hyperpolarizability (β_0) values of **5f**.

Parameters	B3LYP/6-31G (d, p)
Dipole moment (μ) Debye	
μ_x	−1.50
μ_y	−0.97
μ_z	−1.50
μ	**1.80Debye**
Polarizability (α_0) x10^{-30} *esu*	
α_{xx}	459.43
α_{xy}	−48.13
α_{yy}	310.52
α_{xz}	−27.49
α_{yz}	−45.21
α_{zz}	306.67
α_0	**0.87 × 10^{-30} esu**
Hyperpolarizability (β_0) x10^{-30} *esu*	
β_{xxx}	1080.10
β_{xxy}	−703.01
β_{xyy}	209.89
β_{yyy}	196.20
β_{xxz}	109.30
β_{xyz}	142.81
β_{yyz}	−241.57
β_{xzz}	−48.84
β_{yzz}	154.81
β_{zzz}	40.02
β_0	**11.17 × 10^{-30} esu**

Standard value for urea (μ = 1.3732 Debye, β_0 = 0.3728 × 10^{-30} esu): **esu**-electrostatic unit.

electron acceptor groups. The smaller band gap energy may increase the NLO properties of the molecule. The physical properties of these conjugated molecules are governed by the high degree of electronic charge delocalization along the charge transfer axis and by the low band gaps. The calculated hyperpolarizability of **5f** (β_0 = 11.17 × 10^{-30} esu) is nearly thirty times greater than urea (β_0 = 0.37 × 10^{-30} esu). So, we concluded that the title molecule has better nonlinear optical properties.

3.8. Molecular docking studies

A comparative and automated docking study with newly synthesized lead compounds was performed to determine the best in silico conformation. Crystal structure of human folate receptor alpha in complex with folic acid was taken as the target receptor. The Crystal structure of human folate receptor alpha in complex with folic acid was obtained from Protein Data Bank (http://www.pdb.org/pdb/home/home.do).

Docking of synthesized ligands with 1JIJ exhibit bonds with amino acids present in the active pocket of the receptor. Eleven molecules were considered for docking studies of which seven were synthesized molecules and the remaining one were standards. Docked 2D images of compound **5a** and standard drug were shown in Fig. 6. Best ligand pose energy, wander walls interaction, Pi-Pi interaction, alkyl and Pi-alkyl interaction of all the docked compounds including standard drugs were presented in Table 5. The best ligand pose energy ranging of compound **5a-j** is −15.02–11.82 kcal/mol while the standard drug molecule is −8.85 kcal/mol. In the binding mode, compound **5a, 5b and 5c** was attractively bound to 1JIJ via wander walls interaction, carbon hydrogen bond, Pi-sigma, Pi-cation, Pi-Pi stacked, alkyl and Pi-alkyl interaction. In compound **5a** surrounded by wander walls interaction of amino acids residues ILE172, PHE136, GLY129, GLY74, THR75, THR169, TYR165, THR166, ILE131. The MET77, ARG125, LEU128 and LEU173 amino acids interact in alkyl and Pi-alkyl interaction with imidazole ring and two phenyl rings.

In compound **5b** enclosed by LEU133, ILE172, PHE136, GLY74, TYR170 and THR169. Two amino acids like ILE176, LEU128 interact with imidazole one phenyl and thiophene ring in alkyl and Pi-alkyl interaction. ILE131, ILE78 residues interaction with thiophene and one phenyl ring in Pi-sigma interaction and also pi-pi interaction in methoxy substituted phenyl ring with TYR165 amino acids. ASN124, GLY74, THR75, ILE78, THR169, TYR165, LEU137, SER132 and ILE172 residues enclosed by wander walls interaction in compound 5c. amino acid residues like LEU133, PHE136, ILE176 and leu173 attracted in two phenyl ring and SCH_3 atom with alkyl and pi-alkyl interaction. Only one PHE136 residues well with Pi-cation interaction in imidazole nitrogen atom and Pi-pi stacked interaction with phenyl ring. The two amino acids ILE131 and LEU173 is well with phenyl ring in Pi-Sigma interaction. But, the standard drug molecule are enclosed with wander walls interaction with GLY309, LYS305, VAL303, GLU302, PHE271, LEU55 and GLU112 amino acids. Two residues like ASN109 and ARG58 is attracted with conventional hydrogen bond in some hydroxyl group and amine group with different bond distance. Only one pi alkyl, pi-sigma, Pi-donor hydrogen bond. Standard drug molecules only less interactions compared to compound **5a, 5b** and **5c.** This ensured the binding affinity and results in an increased 1JIJ inhibitory activity compared to standard drug molecule. The results furnished that the compounds **5a, 5b** and **5c** have competency to inhibit **1JIJ** protein and thus have high potential to act as antibacterial agents. The 2D and 3D view of remaining compounds are shown in S4 (Fig. 4. Supplementary information).

3.9. Antimicrobial evaluation

The synthesized compounds **(5a-5j)** were tested for their antibacterial activity against bacterial strains: *Staphylococcus aureus, Streptococcus pyogenes, Shigella flexneri, proteus mirabilis* and *vibrio cholerae* by disc diffusion method. The Zone of inhibition and MICs (Minimum Inhibitory Concentrations) of the compounds against these bacterial strains were reported in Table 6. The compounds **5a** (MIC = 3.125 g/mL) and **5c** (MIC = 3.125 g/mL) exhibited extremely high inhibitory activity against *S. aureus* compared to standard methycillin drug with MIC values of 6.25 g/mL. In compound **5c** the methyl group is strongly bonded with the sulphur atom and also

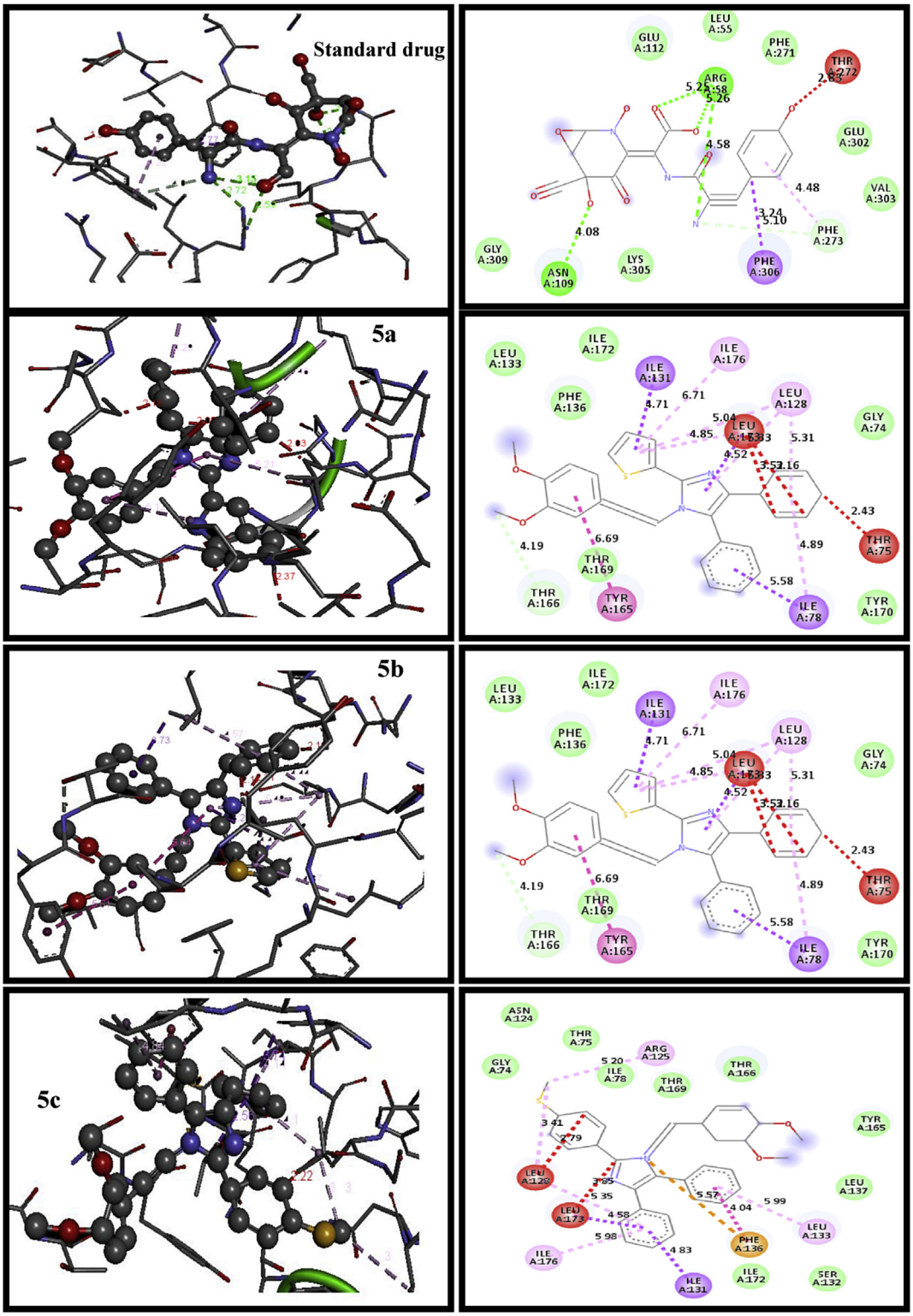

Fig. 6. 3D and 2D View of interaction of compounds (**5a, 5b and 5c**) and standard drug.

Table 5
Different types of interaction of compounds **5a-j** with **1JIJ**.

Compounds	Best ligand pose energy	Vander walls interaction	Alkyl and pi-alkyl interaction	Pi-pi T shaped	Other interactions
5a	−14.56	ILE172, PHE136, GLY129, GLY74,THR75, THR169, TYR165, THR166, 1LE131	MET77, ARG125, LEU128, LEU173	–	–
5b	−14.34	LEU133, ILE172, PHE136, GLY74, TYR170, THR169	ILE176, LEU128,	TYR165	ILE131(Pi-sigma), THR166 (Carbon hydrogen bond)
5c	−15.02	ASN124, GLY74, THR75, ILE78, THR169, TYR169, LEU137, SER132, ILE172	LEU133, PHE136,ILE176,LEU128,	PHE136	PHE136 (Pi-cation), ILE131 (Pi-sigma)
5d	−13.99	THR166, TYR165, 1LE172, THR169,	ILE78, LEU133, LEU128,LEU173		ILE131 (Pi-sigma), PHE136 (Pi-Loan pair)
5e	−13.87	TYR165, LEU137, ILE172, TYR140, GLY73, GLY129, ARG125, GLY74, MET77, THR75, THR166	LEU133, LEU128, LEU173, ILE78	PHE136	ILE131 (Pi-sigma)
5f	−11.88	SER164	LEU159, ILE155, ILE163,PHE168, TYR165, VAL146	TYR165	VAL146 (Pi-sigma)
5g	−13.40	GLY129, MET77, GLY73, ASN124, THR75, THR169, TYR165	ILE131, LEU173, ARG125, PHE136	LEU128 (Amide-Pistacked)	ILE172 (Halogen-F), ILE78, LEU173 (Pi-sigma), THR166 (Carbon hydrogen bond)
5h	−12.63	LEU137, LEU133, ILE172, ILE176, ILE131, LEU128	ILE78, LEU173,	TYR165	THR169 (Pi-sigma), PHE136
5i	−12.17	ARG125, GLY129, GLY74, THR75, ILE78, ILE172, LEU137, THR169, TYR165	ILE131, LEU128, LEU133	PHE136	LEU173 (Pi-sigma), PHE136 (Pi-cation), LEU128 (Carbon hydrogen bond)
5j	−11.82	PHE136, GLY73, LEU90, THR166, THR169,	LEU173, ILE176, ARG125	–	ILE78, ILE131 (Pi-sigma), GLY74, MET77 (Carbon hydrogen bond)
Standard Drug (1JIJ)	−8.85	GLY309, LYS305, VAL303, GLU302, PHE271, LEU55, GLU112	PHE273	–	ASN109, ARG58 (Conventional hydrogen bond), PHE306 (Pi-sigma), PHE273 (Pi-donor hydrogen bond)

Table 6
Zone of inhibition and Minimum inhibitory concentrations of antibacterial activities of compounds **5a-5j**.

Compounds	Zone of inhibition					Minimum inhibitory concentrations. (μg ml^{-1})				
	S. aureus	*S. Pyogenes*	*S. flexneri*	*P. mirabilis*	*V. cholerae*	*S. aureus*	*S. Pyogenes*	*S. flexneri*	*P. mirabilis*	*V. cholerae*
5a	30	24	21	22	18	3.12	6.25	12.5	12.5	25
5b	28	26	19	21	17	6.25	6.25	12.5	12.5	12.5
5c	26	23	20	23	18	3.12	12.5	12.5	12.5	25
5d	28	27	26	25	20	6.25	12.5	12.5	12.5	25
5e	27	25	22	19	21	6.25	6.25	6.25	6.25	12.5
5f	26	26	23	20	19	6.25	6.25	12.5	12.5	25
5g	25	24	20	20	16	6.25	6.25	12.5	25	25
5h	26	26	23	18	20	6.25	6.25	12.5	25	12.5
5i	10	10	11	8	8	25	25	25	25	25
5j	9	10	10	8	8	25	25	25	25	25
Methicilin	20	19	19	21	20	6.25	6.25	6.25	6.25	6.25

Table 7
Zone of inhibition and Minimum inhibitory concentrations of antifungal activities of compounds **5a-5j**.

Compounds	Zone of inhibition			Minimum inhibitory concentrations. (μg ml^{-1})		
	C. albicans	*C. glubrate*	*C. crusei*	*C. albicans*	*C. glubrate*	*C. crusei*
5a	10	10	11	25	50	25
5b	9	8	11	25	25	12.5
5c	8	8	10	25	25	25
5d	11	11	12	50	50	25
5e	9	11	12	25	25	12.5
5f	11	10	10	25	25	25
5g	10	8	11	25	25	25
5h	10	10	12	25	25	12.5
5i	8	6	10	50	50	50
5j	8	6	8	50	50	50
Amphotercin B	14	14	14	12.5	12.5	12.5

the aromatic amine having two methoxy groups hence the inhibitory activity may increases. Compound **5b** (MIC = 6.25 g/mL) exhibited the same activity with the standard drug against *S. aureus and S. Pyogenes.* The synthesized compounds **5d-5h** exhibited same activities against *S. aureus* and *S. pyogenes* with standard drug and moderate inhibitory activities against *S. flexneri, P. mirabilis and V. cholerae.* The compound **5e** is also exhibited equivalent activity as compared with standard drug against *S. aureus, S. Pyogenes, S. flexneri and P. mirabilis.* The compound **5i** and **5j** exhibited only moderate activities against all the bacterial strains. At the outset,

the trend of the antibacterial activity of all the compounds is as follows: **5a** > **5c** > **5b** > **5e** > **5f** > **5g** > **5h** > **5d** > **5i** > **5j.**

The synthesized compounds were also tested for their antifungal activity against *Candida albicans, Candida glubrate* and *Candida crusei* by disc diffusion method. The zone of inhibition and MICs (Minimum Inhibitory Concentrations) of the compounds against these fungal were reported in Table 7. These results revealed that the compounds **5b** (MIC = 12.5 g/mL), **5e** (MIC = 12.5 g/mL) and **5h** (MIC = 12.5 g/mL) showed equivalent activity against *Candida crusei* as compared to standard Amphotericin B with MIC value of 12.5 g/mL. Most of the compounds exhibited good and moderate inhibitory activities against *Candida albicans, Candida glubrate* and *Candida crusei.* The Minimum inhibitory concentrations (μg ml^{-1}) of compounds **5a-5j** in antibacterial and antifungal activity are shown in S5 and S6 (Supplementary information).

4. Conclusion

In summary, we have synthesized a series of ten 3-(1-(3,4-dimethoxyphenethyl)-4,5-diphenyl-*1H*-imidazol-2-yl)-*1H*-indole derivatives. The complete vibrational spectral analysis of **5f** was performed by combining the experimental and hypothetical information obtained using density functional theory. The DFT/B3LYP method with 6−31G (d, p) level of theory showed better agreement with the experimental data. The most important interaction energies of charge transfer are mainly by the orbital overlap between n (LP- N5) and π*C3−N4 with stabilization energy of 197.86 kJ/mol and electron density 1.55e which results intramolecular charge transfer (ICT) causing stabilization of the system. HOMO−LUMO energy gap with 4.38eV indicates that the compound **5f** has a good chemical stability and reactivity. Atomic charges on the various atoms of **5f** obtained by mulliken population analysis. It was also observed that there is a large accumulation of positive charge on C3 and C52 atoms. The large negative charges are accumulated on N5, O54 and O59 in the molecule. The reported compound **5f** used as a potential NLO material since it has high $\mu\beta_0$ value. All the compounds evaluated for their in vitro antimicrobial activities. Antibacterial and antifungal activities revealed that the compound **5a** (MIC = 3.125 g/mL) and **5c** (MIC = 3.125 g/mL) exhibited extremely high inhibitory activities against *S. aureus* compared to standard methycillin drug with MIC values of 6.25 g/mL. Compounds **5b** (MIC = 12.5 g/mL), **5e** (MIC = 12.5 g/mL) and **5h** (MIC = 12.5 g/mL) showed equivalent activity against *Candida crusei* compared to standard Amphotericin B. The molecular docking results clearly specify that the tested analogues demonstrate polar, hydrophobic, pi-pi interactions with different amino acids present in the active site of **1JIJ**. The results furnished that the compounds **5a, 5b** and **5c** have competency to inhibit **1JIJ** protein and thus have high potential to act as antibacterial agents.

Acknowledgements

The authors Dr. K. Krishnasamy and D. Rajaraman thank the university grant commission for the financial support (Major Research Project, F. NO: 42-342/2013) of this research work. Authors are thankful to Dr. N. K. Lokanath, Department of Studies and Physics, University of Mysore for his help in the Crystallographic study. The authors extended thankful to Department of Botany, Annamalai University for carrying out the antimicrobial activities.

Appendix A. Supplementary data

Supplementary data related to this article can be found at http://dx.doi.org/10.1016/j.molstruc.2016.08.021.

References

[1] J.R. Coura, S.L. De Castro, A critical review on chagas disease chemotherapy, Mem. Inst. Oswaldo Cruz 97 (2002) 3–24.
[2] A. Saeed, M. Batool, Synthesis and bioactivity of some new 1-tolyl-3-aryl-4-methylimidazole-2-thiones, Med. Chem. Res. 16 (2007) 143–154, http://dx.doi.org/10.1007/s00044-007-9017-8.
[3] P. Franchetti, L.S. Marchetti, J.A. Cappaellaci, H.N. Yalowitz, B.M. Jayaram, M. Glodstein, A. Grafantini, Synthesis, conformational analysis, and biological activity of Thioribonucleosides related to Tiazofurin, Bioorg. Med. Chem. Lett. 11 (1) (2001) 67–69.
[4] T. Nakamura, H. Kakinuma, H. Umemiya, H. Amada, N. Miyata, K. Taniguchi, K. Bando, M. Sato, Imidazole derivatives as new potent and selective 20-HETE synthase inhibitors, Bioorg. Med. Chem. Lett. 14 (2) (2004) 333–336.
[5] A.M. Venkatesan, A. Agarwal, T. Abe, H. Ushirogochi, O.D. Santos, A. Mihira, T. Takasaki, G. Francisco, Y.I. Lin, P.J. Peterson, Y. Yang, W.J. Weiss, D.M. Shales, T.S. Mansour, Structure-activity relationship of 6-Methylidene penems bearing 6,5 bicyclic heterocycl as broad-spectrum β-lactamase inhibitors: evidence for 1,4-Thiazepine intermediates with C7 R Stereochemistry by computational methods, Bioorg. Med. Chem. 16 (2008) 1890.
[6] M.S. Han, D.H. Kim, Effect of zinc ion on the inhibition of carboxypeptidase A by imidazole bearing substrate analogues, Bioorg. Med. Chem. Lett. 11 (2001) 1425–1427.
[7] G. Roman, J.G. Riley, J.Z. Vlahakis, R.T. Kinobe, J.F. Brien, K. Nakatsu, W.A. Szarek, Heme oxygenase inhibition by 2-oxy-substituted 1-(1H-imidazol-1-yl)-4- phenylbutanes: effect of halogen substitution in the phenyl ring, Bioorg. Med. Chem. 15 (2007) 3225–3234.
[8] P.G. Nantermet, J.C. Barrow, S.R. Lindsley, M. Young, S. Mao, S. Carroll, C. Bailey, M. Bosserman, D. Colussi, D.R. McMasters, J.P. Vacca, H.G. Selnick, Imidazole acetic acid TAFIa inhibitors: SAR studies centered around the basic P(1)(') group, Bioorg. Med. Chem. Lett. 14 (2004) 2141–2145, http://dx.doi.org/10.1016/j.bmcl.2004.02.033.
[9] V. Sorrenti, L. Salerno, C.D. Giacomo, R. Acquaviva, M.A. Siracusa, A. Vanella, Imidazole derivatives as antioxidants and selective inhibitors of nNOS, Nitric Oxide 14 (2006) 45–50.
[10] E.C. Power, C.R. Ganellin, D.C. Benton, Artial structures of ketoconazole as modulators of the large conductance calcium-activated potassium channel, Bioorg. Med. Chem. Lett. 16 (2006) 887–890, http://dx.doi.org/10.1016/j.bmcl.2005.11.001.
[11] J.L. Adams, J.C. Boehm, T.F. Gallagher, S. Kassis, E.F. Webb, R. Hall, M. Sorenson, R. Garigipati, D.E. Griswold, J.C. Lee, Pyrimidinylimidazole inhibitors of p38: cyclic N- imidazole substituents enhance p38 kinase inhibition and oral activity, Bioorg. Med. Chem. Lett. 11 (2001) 2867–2870.
[12] D. Rajaraman, G. Sundararajan, R. Rajkumar, S. Bharanidharan, K. Krishnasamy, Synthesis, crystal structure investigation, DFT studies and DPPH radical scavenging activity of 1-(furan-2-ylmethyl)-2,4,5-triphenyl-1H-imidazole derivatives, J. Mol. Struct. 1108 (2016) 698–707.
[13] T. Mano, R.W. Stevens, K. Ando, K. Nakao, T. Okumura, M. Sakakibara, T. Okumura, T. Tamura, K. Miyamoto, Novel imidazole compounds as a new series of potent, orally active inhibitors of 5-lipoxygenase, Bioorg. Med. Chem. 11 (2003) 3879–3887, http://dx.doi.org/10.1016/S0968-0896(03)00436-X.
[14] V.K. Gore, V.V. Ma, R. Tamir, N.R. Gavva, J.J. Treanor, M.H. Norman, Structure-activity relationship (SAR) investigations of substituted imidazole analogs as TRPV1 antagonists, Bioorg. Med. Chem. Lett. 17 (2007) 5825–5830, http://dx.doi.org/10.1016/j.bmcl.2007.08.044.
[15] L. Navidpour, H. Shadnia, H. Shafaroodi, M. Amini, A.R. Dehpour, A. Shafiee, Design, synthesis, and biological evaluation of substituted 2-alkylthio-1,5-diarylimidazoles as selective COX-2 inhibitors, Bioorg. Med. Chem. 15 (2007) 1976–1982.
[16] S. Khabnadideh, Z. Rezaei, A. Khalafi-Nezhad, R. Bahrinajafi, R. Mohamadi, A.A. Farrokhroz, Synthesis of N-alkylated derivatives of imidazole as antibacterial agents, Bioorg. Med. Chem. Lett. 13 (2003) 2863–2865.
[17] A.K. Saha, L. Liu, P. Marichal, F. Odds, Novel antifungals based on 4-substituted imidazole: solid-phase synthesis of substituted aryl sulfonamides towards optimization of in vitro activity, Bioorg. Med. Chem. Lett. 10 (2000) 2735–2739.
[18] A.K. Saha, L. Liu, R.L. Simoneaux, M.J. Kukla, P. Marichal, F. Odds, Novel antifungals based on 4-substituted imidazole: a combinatorial chemistry approach to lead discovery and optimization, Bioorg. Med. Chem. Lett. 10 (2000) 2175–2178.
[19] R.K. Ujjinamatada, A. Baier, P. Borowski, R.S. Hosmane, n analogue of AICAR with dual inhibitory activity against WNV and HCV NTPase/helicase: synthesis and in vitro screening of 4-carbamoyl-5-(4,6-diamino-2,5-dihydro-1,3,5-triazin-2-yl)imidazole-1-beta-D-ribofuranoside, Bioorg. Med. Chem. Let. 17 (2007) 2285–2288.
[20] D. Zampieri, M.G. Mamolo, L. Vio, E. Banfti, G. Scialino, M. Fermeglia, M. Ferrone, S. Pricl, Antifungal and antimycobacterial activity of 1-(3,5-diaryl-4,5-dihydro-1H-pyrazol-4-yl)-1H-imidazole derivatives, Bioorg. Med. Chem. 15 (2007) 7444–7458, http://dx.doi.org/10.1016/j.bmc.2007.07.023.
[21] S.B. Ferreira, M.S. Costa, N. Boechat, R.J.S. Bezerra, M.S. Genestra, M.M. Canto Cavalheiro, W.B. Kover, V.F. Ferreira, Synthesis and evaluation of new difluoromethyl azoles as antileishmanial agents, Eur. J. Med. Chem. 42 (2007) 1388–1395, http://dx.doi.org/10.1016/j.ejmech.2007.02.020.
[22] M. Kawanishi, N. Kotoku, S. Itagaki, T. Horii, M. Kobayashi, Structure-activity

relationship of anti-malarial spongean peroxides having a 3-methoxy-1,2-dioxane structure, Bioorg. Med. Chem. 12 (2004) 5297–5307, http://dx.doi.org/10.1016/j.bmc.2004.04.051.
[23] D. Riddell, C.P. Bright, B.J. Burton, R.C. Bush, N.V. Harris, D. Hele, U.M. Moore, K. Naik, D.P. Parrott, C. Smith, R.J. Williams, Hypolipidaemic properties of a potent and bioavailable alkylsulphinyl-diphenylimidazole ACAT inhibitor (RP 73163) in animals fed diets low in cholesterol, Bio Chem. Pharmacol. 52 (1996) 1177–1186, http://dx.doi.org/10.1016/0006-2952(96)00455-8.
[24] R.W. Clarke, J. Harris, RX 821002 as a tool for physiological investigation of alpha(2)-adrenoceptors, CNS Drug Rev. 8 (2002) 177–192.
[25] U. Ucucu, N.G. Karaburun, I. Isikdag, Synthesis and analgesic activity of some 1-benzyl- 2-substituted-4,5-diphenyl-1H-imidazole derivatives, Farmaco 56 (2001) 285–290.
[26] J.W. Black, J.G. Durant, J.C. Emmett, C.R. Ganellin, Sulphur-methylene isosterism in the development of metiamide, a new histamine H2-receptor antagonist, Nature 248 (1974) 65–67.
[27] L. Wang, K.W. Woods, Q. Li, K.J. Barr, R.W. McCroskey, S. Hannick, L.M. Gherke, R.B. Credo, Y.H. Hui, K. Marsh, R. Warner, J.Y. Lee, N.D. Zielinski-Mozng, S.H. Frost, H.L. Rosenberg Sham, Potent, orally active heterocycle-based combretastatin A-4 analogues: synthesis, structure-activity relationship, pharmacokinetics and in vivo antitumor activity evaluation, J. Med. Chem. 45 (2002) 1697–1711, http://dx.doi.org/10.1021/jm010523x.
[28] G.K. Sharma, D. Pathak, Microwave-assisted, solvent-free and parallel synthesis of some novel substituted imidazoles of biological interest, Chem. Pharm. Bull. 58 (3) (2010) 375–380, http://dx.doi.org/10.1248/cpb.58.375.
[29] G.L. Praveena, T. Balu, R. Sreedevi, Growth and characterization of imidazole potassium chloride – a semiorganic NLO crystal, Int. J. ChemTech. Res. 8 (3) (2015) 1338–1345.
[30] R. Schmierer, H. Mildenberger, H. Buerstell, ChemAbstr 108 (1998) 8939–8942.
[31] M. Velusamy, Y.C. Hsu, J.T. Lin, C.W. Chang Hsu, 1-Alkyl-1H-imidazole-based dipolar organic compounds for dye-sensitized solar cells, Chem. Asian J. 5 (2010) 87–96, http://dx.doi.org/10.1002/asia.200900244.
[32] D. Kumar, K.R. Justin Thomas, Ching-Chiao Lin, Jwo-Huei Jou, Pyrenoimidazole-based deep blue emitting materials: optical, electrochemical and electroluminescent characteristics, Chem. Asian J. 8 (2013) 2111–2124.
[33] D.N. Sathyanarayana, Vibrational Spectroscopy Theory and Applications, Seconded, New Age International (P) Limited Publishers, New Delhi, 2004.
[34] M.J. Frisch, Gaussian 03 Program, Gaussian Inc., Wallingford, CT, 2004.
[35] R. Rajkumar, A. Kamaraj, K. Krishnasamy, Synthesis, spectral characterization and biological evaluation of novel 1-(2-(4,5-dimethyl-2-phenyl-1H-imidazol-1- yl)ethyl)piperazine derivatives, J. Saudi Chem. Soc. 18 (2014) 735–743, http://dx.doi.org/10.1016/j.jscs.2014.08.001.
[36] H.B. Schlegel, Optimization of equilibrium geometries and transition structures, J. Comput. Chem. 3 (1982) 214–218, http://dx.doi.org/10.1002/jcc.540030212.
[37] G. Rauhut, P. Pulay, Transferable scaling factors for density functional derived Vibrational Force Fields, J. Phys. Chem. 99 (1995) 3093–3100, http://dx.doi.org/10.1021/j100010a019.
[38] G. Keresztury, J.M. Chalmers, P.R. Griffith, Raman Spectroscopy: Theory, Hand Book of Vibrational Spectroscopy, vol. 1, John Wiley & Sons Ltd, New York, 2002.
[39] G. Keresztury, S. Holly, J. Varga, G. Besenyei, A.Y. Wang, J.R. Durig, Vibrational spectra of monothiocarbamates-II. Ir and raman spectra, vibrational assignment, conformational analysis and ab initio calculations of S-Methyl-N,N-dimethylthiocarbamate, Spectrochim. Acta 49 (1993) 2007–2026, http://dx.doi.org/10.1016/S0584-8539 (09) 91012–1.
[40] S.D. Sharma, P. Hazarika, D. Konwar, An efficient and one pot synthesis of 2,4,5- trisubstituted and 1,2,4,5-tetrasubstitutedimidazoles catalyzed by $InCl_3 \cdot 3H_2O$, Tetrahedron Lett. 49 (2008) 2216–2220.
[41] M. Tahir Gulluoglu, Y. Erdogdu, S. Yurdakul, Molecular structure and vibrational spectra of piperidine and 4-methylpiperidine by density functional theory and ab initio Hartree–Fock calculations, J. Mol. Struct. 834 (2007) 540–547.
[42] Y. Erdogdu, M.T. Gulluoglu, Analysis of vibrational spectra of 2 and 3-methylpiperidine based on density functional theory calculations, Spectrochim. Acta 74A (2009) 162–167, http://dx.doi.org/10.1016/j.saa.2009.05.025.
[43] Y.R. Sharma, Elementary Organic Spectroscopy Principles and Chemical Applications, S. Chand & Company Ltd, New Delhi, 1994.
[44] N.P.G. Roeges, A Guide to the Complete Interpretation of Infrared Spectra of Organic Structure, Wiley, New York, 1994.
[45] A.E. Reed, F. Weinhold, Natural localized molecular orbitals, J. Chem. Phys. 83 (1985) 1736–1740, http://dx.doi.org/10.1063/1.449360.
[46] B. Smith, Infrared Spectral Interpretation: a Systemic Approach, CRC, Washington, DC, 1999.
[47] A.E. Reed, F. Weinhold, Natural bond orbital analysis of near-Hartree–Fock water dimer, J. Chem. Phys. 78 (1983) 4066–4073.
[48] M. Alcolea palafox, Scaling factors for the prediction of vibrational spectra. I. Benzene molecule, Int. J. Quantum Chem. 77 (2000) 661–684, http://dx.doi.org/10.1002/(SICI)1097-461X(2000)77, 3<661::AID-QUA7>3.0.CO;2-J.
[49] P. Agarwal, S. Bee, A. Gupta, P. Tandon, V.K. Rastogi, S. Mishra, Quantum chemical study on influence of intermolecular hydrogen bonding on the geometry, the atomic charges and the vibrational dynamics of 2, 6-dichlorobenzonitrile, Spectrochem. Acta A 121 (2014) 464–482.
[50] S. Gunasekaran, S. Kumaresan, R. Arunbalaji, G. Anand, S. Srinivasan, Density functional theory study of vibrational spectra, and assignment of fundamental modes of dacarbazine, J. Chem. Sci. 120 (2008) 315–324.
[51] R.S. Mulliken, Electronic population analysis on LCAO–MO molecular wave functions, J. Chem. Phys. 23 (1955) 1833–1840, http://dx.doi.org/10.1063/1.1740588.